ELEMENTA
Science of the Anthropocene

Smyth, TJ, et al. 2022. Disruption of marine habitats by artificial light at night from global coastal megacities. *Elem Sci Anth*, 10: 1. DOI: https://doi.org/10.1525/elementa.2022.00042

RESEARCH ARTICLE

Disruption of marine habitats by artificial light at night from global coastal megacities

T. J. Smyth[1,*], A. E. Wright[1], A. Edwards-Jones[1], D. McKee[2,3], A. Queirós[1], O. Rendon[1], S. Tidau[4], and T. W. Davies[4]

Half of globally significant megacities are situated near the coast, exposing urban marine ecosystems to multiple stressors such as waste-water discharge containing a host of organic and inorganic pollutants, air and noise pollution. In addition to these well recognized sources, artificial light at night (ALAN) pollution is inseparable from cities but poorly quantified in marine ecosystems to date. We have developed a time- and wavelength-resolving hydrological optical model that includes solar (daylight and twilight components), lunar and ALAN source terms and propagates these spectrally through a tidally varying water column using Beer's Law. Our model shows that for 8 globally distributed cities surface ALAN dosages are up to a factor of 6 greater than moonlight, as ALAN intensities vary little throughout the night, over monthly or seasonal cycles. Moonlight only exceeds ALAN irradiances over the ±3-day period around full moon, and particularly during the brightest moons (mid-latitude winter, at zenith). Unlike the relatively stable surface ALAN, underwater ALAN varies spectrally and in magnitude throughout the night due to tidal cycles. The extent of ALAN in-water attenuation is location-specific, driven by the season, tidal range and cycle, and water clarity. This work highlights that marine ALAN ecosystem pollution is a particularly acute global change issue near some of the largest cities in the world.

Keywords: Artificial light at night, Tidal cycle, Hydrological optical model, Radiative transfer modelling, Urban marine ecosystems, Coastal megacities

Introduction

Before the Anthropocene, and indeed before the Urbanocene (West, 2018) in the past 50–100 years, light at astronomical night was governed by the moon and its cycle of waxing, waning and elevation in the sky. Increasing urbanization and associated artificial light at night (ALAN) are disrupting natural light cycles and biological adaptations to them from the hyperlocal (underneath street-lights) to regional and global scales (e.g., Smyth et al., 2021; Tidau et al., 2021). Satellite observations show clearly the global pervasiveness of ALAN urban environments (Falchi et al., 2016), and many of the world's megacities are located near the coast (United Nations, 2019). The recent global atlas of underwater ALAN shows the extent of ALAN in coastal-marine ecosystems (Smyth et al., 2021) covering over 1.9 million km^2 of the world's coastal seas. In short, ALAN pollution is widespread (Davies et al., 2014), pervasive and expanding in its reach (Gaston et al., 2021) and should therefore be recognized as a major 21st century global anthropogenic change issue (Davies and Smyth, 2018).

ALAN impacts range from altering organismal physiology to changes wrought in ecological communities (Sanders et al., 2021). Underwater ALAN affects multiple aspects of the life histories of marine organisms, including reducing reproductive success in fish (Fobert et al., 2019; Fobert et al., 2021) and turtles (Witherington and Bjorndal, 1991); disrupting migration in zooplankton (Ludvigsen et al., 2018; Berge et al., 2020) and sandhoppers (Torres et al., 2020); altering recruitment in marine epifaunal communities (Davies et al., 2015); shifting interspecific interactions in estuarine fish (Becker et al., 2013), symbiotic reef building corals (Levy et al., 2020), and intertidal invertebrates (Underwood et al., 2017); delaying coral gametogenesis (Ayalon et al., 2021); and changing phytoplankton abundance (Diamantopoulou et al., 2021). For a recent review of the impacts of ALAN in marine ecosystems, see Marangoni et al. (2022).

The amount of visible light entering the underwater marine habitat is governed in the first instance by the intensity and spectral distribution of the above-water

[1] Plymouth Marine Laboratory, Plymouth, Devon, UK
[2] Physics Department, University of Strathclyde, Glasgow, UK
[3] Department Arctic and Marine Biology, Faculty for Bioscience, Fisheries and Economy, UiT The Arctic University of Norway, Tromsø, Norway
[4] School of Biological and Marine Sciences, University of Plymouth, Plymouth, UK

* Corresponding author:
Email: tjsm@pml.ac.uk

Downloaded from http://online.ucpress.edu/elementa/article-pdf/10/1/00042/765092/elementa.2022.00042.pdf by University of Strathclyde Glasgow user on 13 December 2022

source, whether natural (solar, lunar) or artificial, for example, light-emitting diode (LED), low pressure sodium (LPS), and high pressure sodium (HPS). Natural sources have well understood seasonal cycles, governed by their altitude (and phase for the moon), which is a function of latitude, longitude, day of year and time of day (night). By contrast, artificial light sources have a fixed position, giving the same intensity throughout the night (neglecting the effects of changes in cloud cover, base height and type of artificial skyglow). In simple terms, natural sources describe sinusoidal behavior, whereas anthropogenic sources are best described by a "top-hat" function, a binary "on-off." Once the light has penetrated the water, it is rapidly attenuated with depth: the rate of attenuation is a complex function of wavelength that is dependent upon the in-water inherent optical properties (IOPs; Lee et al., 2002) which, in turn, exhibit strong spatio-temporal variability (Mobley, 1994). For a complete description of ALAN exposure in marine habitats of relatively shallow waters (<10 m), such as estuaries, beaches and rocky shores, the effects of variable water column depth should also be included (Roberts et al., 2018). These effects further modulate the underwater spectral light field as a function of time, tidal magnitude (14-day spring/neap cycle), location and time of year. Furthermore, large habitat-forming species such as seaweed will likely modulate the underwater lightscape in coastal areas (Gerard, 1984; Dierssen et al., 2015), but data on this effect are still missing (Tidau et al., 2021).

Of the top 25 global megacities (population >10 million), 16 are classified as being coastal (United Nations, 2019). In this paper, we have modelled the light cycles experienced by the adjacent marine environment over an annual cycle (2020), including the relative contributions of natural (solar, twilight, lunar) and ALAN sources for these global megacity locations, and quantified their instantaneous spectral irradiances as well as the significance of longer term monthly–seasonal exposure. Our model enabled a first quantification of the relative intensities and dosages of natural and anthropogenic light at the surface and within the tidal range, allowing important metrics of this emergent environmental stressor to be determined for key globally significant urban areas.

Method

In order to give a worldwide geographical spread, we selected the following megacities (in order of population size): Tokyo (Japan, 37 million), Shanghai (China, 26 million); Mumbai (India, 20 million); New York (USA, 19 million); Buenos Aires (Argentina, 15 million); Lagos (Nigeria, 13 million); and Los Angeles (USA, 12 million). We also calculated the relative natural and anthropogenic contributions for Plymouth (UK, 234 thousand), a city for which biologically important (Båtnes et al., 2015) ALAN levels have been quantified (Davies et al., 2020) and with an established track record in marine ALAN research over an annual (2020) and 20-year (2001–2020) period, the latter to capture variability in intensity as the tidal and celestial harmonics shift in phase over the metonic cycle (approximately 19 years).

Hydrological optical modelling

A generalized modelling framework was developed using the Python programming language in order to simulate the surface and underwater spectral light field as a function of location (latitude, longitude), date, time, tidal range and depth of water overlying an intertidal point. The model required an above-surface component (solar and lunar spectral model, tidal model, ALAN) and an in-water optical component.

Solar spectral model

The top of atmosphere (TOA) spectral solar irradiances, $E_0(\lambda)$, at 1-nm resolution were calculated using a look-up-table (Neckel and Labs, 1984) of the solar spectral irradiance, $H_0(\lambda)$, and corrected for the eccentricity (ε) of Earth's orbit (function of day of year, D) using the equation:

$$E_0(\lambda) = H_0(\lambda)\left(1 + \varepsilon\cos\left\{\frac{2\pi(D - 3)}{365}\right\}\right)^2 \ (\mathrm{W\ m^{-2}}). \quad (1)$$

The Gregg and Carder (1990) spectral marine atmosphere model was used to determine the spectral (just) above-surface solar irradiance, assuming clear sky conditions. This model is relatively simple but does consider gaseous absorption and aerosol optical properties and allows for the partitioning of the irradiance field into direct, $E_{dd}(\lambda)$, and diffuse, $E_{ds}(\lambda)$, components. The global above-surface spectral irradiance is the sum of these two terms:

$$E_d(\lambda, 0^+) = E_{dd}(\lambda) + E_{ds}(\lambda) \ (\mathrm{W\ m^{-2}}). \quad (2)$$

Additionally, the spectral twilight model of Spitschan et al. (2016) was used to determine the spectral sky (diffuse) irradiance for solar zenith angles (θ_z) between 0° and −18°, using a look-up-table constructed from their rural sky observations. This approach allowed the twilight period to be split between civil ($0° \le \theta_z < -6°$), nautical ($-6° \le \theta_z < -12°$) and astronomical ($-12° \le \theta_z < -18°$) partitions.

Lunar spectral model

The TOA spectral lunar irradiances were determined using the TOA spectral solar irradiances (Equation 1), assuming a lunar albedo of 16% (Buratti et al., 1996) and a lunar semi-diameter view angle of 0.26°. The lunar zenith angle was calculated as a function of location, date and time using the Python astropy (https://pypi.org/project/astropy) package. The phase curve of Lumme and Bowell (1981) was used to account for the full moon brightening, and lunar phase calculated as a function of latitude, date and time using the Python astroplan (https://pypi.org/project/astroplan) package. The Gregg and Carder (1990) model was then used to determine the spectral surface lunar irradiance, assuming clear sky conditions.

The substantive differences between the solar and lunar components are: (a) the magnitude of the TOA

Downloaded from http://online.ucpress.edu/elementa/article-pdf/10/1/00042/765092/elementa.2022.00042.pdf by University of Strathclyde Glasgow user on 13 December 2022

irradiance (Equation 1), which for the lunar component is roughly five orders of magnitude less than the solar for a full moon; (b) the phase of the moon; and (c) their respective celestial geometries (i.e., position in the sky).

ALAN source term

The above-surface ALAN spectral irradiances can be generally derived from spectral shape functions for a given lighting source (e.g., LED, HPS, LPS) and scaled by a reasonable/informed factor to give an intensity. In this paper we used the approach outlined in Smyth et al. (2021) validated against data originally reported in Tamir et al. (2017), where the above-surface sky brightness (Falchi et al., 2016) for a given city location is spectrally resolved into blue ($E(\lambda)_b$ 400–500 nm), green ($E(\lambda)_g$ 495–560 nm) and red ($E(\lambda)_r$ 620–740 nm) broad wavelength bands based on empirical field data collected close to the city of Plymouth, UK (Davies et al., 2020).

In-water optics

The in-water spectral irradiance was determined for a given water depth, z, using Beer's law:

$$E(\lambda, z) = E_d(\lambda, 0^+)\exp(-k_d(\lambda)z) \ \ (\mathrm{W\ m^{-2}}), \qquad (3)$$

where $E_d(\lambda,0^+)$ is the above surface spectral irradiance term and $k_d(\lambda)$ the spectral diffuse attenuation coefficient (m^{-1}). The value of $E_d(\lambda,0^+)$ can be individually compartmentalized into solar, twilight, lunar and ALAN components. During daylight hours ($\theta_z > 0°$), only the solar $E_d(\lambda,0^+)$ was calculated. After sunset, twilight $E_d(\lambda,0^+)$ was calculated for $0° < \theta_z \leq -18°$; ALAN $E_d(\lambda,0^+)$ was calculated when $\theta_z \leq -6°$ (i.e., between civic twilight after sunset and before sunrise); and lunar $E_d(\lambda,0^+)$ was calculated for $0° < \theta_z$ if the moon was above the horizon. In this paper we extracted monthly climatological values of $k_d(\lambda)$ for the given city locations, using the approach of Smyth et al. (2021), which uses an IOP model (Lee et al., 2002) implemented on a global ocean colour dataset (Sathyendranath et al., 2019) to drive a radiative transfer model (Mobley, 1995). The 12 monthly values of spectral k_d (blue, green, red) for each city location are shown in Table S1.

Tidal model

The depth (z) of the water column at a given location was defined as a function of position above the low-tide mark and is strongly determined by tidal variability, which itself is dependent upon the spring-neap cycle and the magnitude of tides experienced at that location. For each coastal city, local tide gauge data were sourced from the University of Hawaii Sea Level Center (http://uhslc.soest.hawaii.edu/data/) or reconstructed from the Oregon State University TOPEX/Poseidon Global Inverse Solution tidal model (Egbert and Erofeeva, 2002; TPXO: https://tpxows.azurewebsites.net/; see Table S2 for specific location details), and the maximum and minimum tide determined. The intertidal point was then defined as 25% of the tidal range of that location, added to the minimum tidal height. For the in-water model to have realistic water depths and be generalizable in time (past and future), the tidal harmonics for each city location were determined from the relevant tide gauge data using the Python utide (V0.2.6) package (https://pypi.org/project/UTide). The utide model was then run using those tidal harmonics to determine the tidal heights for a given date and time.

Model experiments

For each city location (see Table S1 for geographical positions) we ran the model for one calendar year (2020) using a 15-minute timestep to determine the above-surface (0^+) and intertidal point values of $E_d(\lambda, z)$ for the solar, twilight, lunar and ALAN sources. For consistency with Smyth et al. (2021) we used the broad wavelength bands of blue (400–495 nm), green (500–560 nm) and red (620–740 nm) for the spectral components, and integrated over these bands (stepped at 1-m depth intervals) to get the broadband (approximately the photosynthetically available radiation) signal. This approach resulted in approximately 35,000 calculations per location. Additionally, for the city of Plymouth the model was run for 20 calendar years (2001–2020) in order to capture interannual variability over the metonic cycle (approximately 19 years), in order for any variability in the superposition of the lunar and tidal cycles to be quantified (approximately 70,000 calculations).

Results

For illustrative purposes, **Figure 1** shows the shape and magnitude of the various surface irradiance source terms and how they vary for Tokyo (mid-latitude) over one calendar month (January). Unsurprisingly, most variability is shown in the lunar cycle (**Figure 1B**) as the moon waxes and wanes, reaching full moon on day 10 in 2020. The full moon intensity peaks at >1000 $\mu W\ m^{-2}$ when the moon reaches the highest altitude, which is at local midnight. As the moon rises progressively later through the month, there is an observable asymmetrical pattern in the lunar intensity. During daylight the moon is effectively "switched off," contributing five orders of magnitude less light than daylight. For this location at this time of year, the waxing moon is also higher in the sky than the waning moon: this effect is seasonally and latitudinally dependent, with little seasonal variability at low latitudes. As a rough rule of thumb, mid-latitude summer full moons appear lower in the sky than their winter counterparts, with a higher waxing than waning moon towards winter and reversed in the summer. These natural rhythms are in stark contrast to ALAN (**Figure 1C**), where the variability can best be described as a top-hat function with no daily variability. The duration of the ALAN signal is controlled by the variability in sunrise and sunset times, so mid- to high-latitude locations will show the most variability.

The variability in the tidal signal for Tokyo over the same time period (**Figure 2A**) clearly shows the spring-neap cycle, with spring tides occurring around the new and full moon (**Figure 2B**). Tokyo has multiple harmonics associated with its tidal cycle, which results in a double peak at high tide, with the low-tide amplitudes differing. The double-peak is particularly accentuated towards spring tide. As with the lunar cycle, the tidal "day" is not

Downloaded from http://online.ucpress.edu/elementa/article-pdf/10/1/00042/765092/elementa.2022.00042.pdf by University of Strathclyde Glasgow user on 13 December 2022

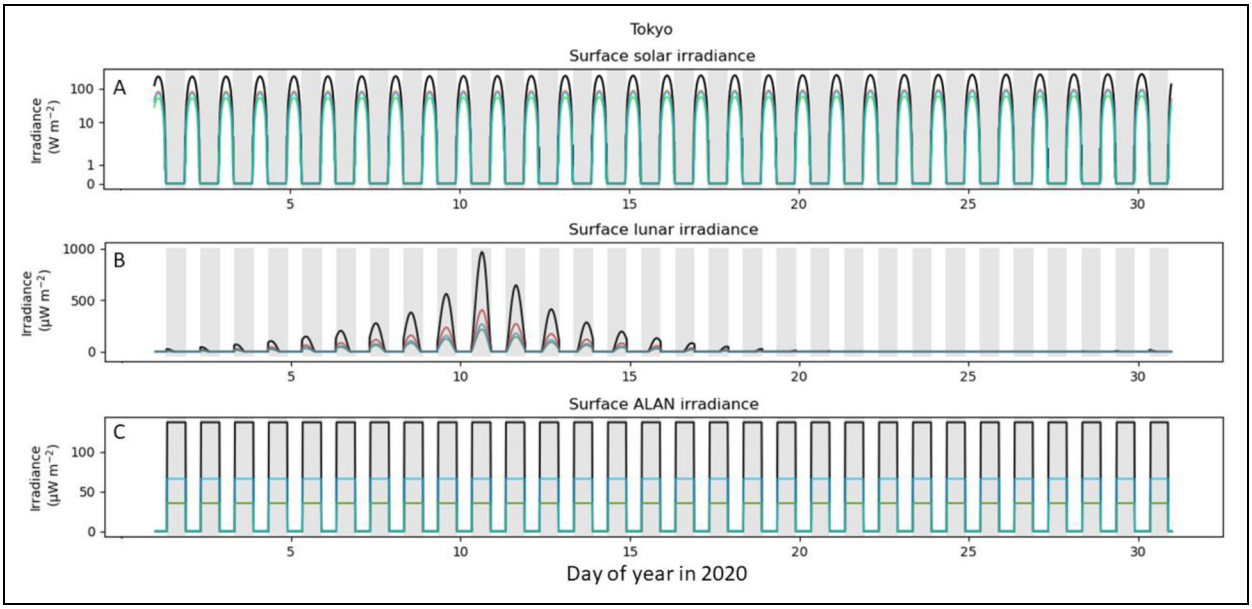

Figure 1. Surface irradiances for Tokyo in January 2020. Spectral irradiances for (A) solar (blue), (B) lunar (green), and (C) artificial light at night (ALAN, red) and broadband (black) irradiances calculated at the surface for Tokyo over two tidal cycles (day of year 001–031; January 1–31, 2020). Night-time periods are shaded in gray. Solar irradiance is on a logarithmic scale (W m^{-2}); lunar and ALAN, a linear scale (μW m^{-2}). Times (start of day) on x-axis are in GMT: Tokyo is GMT + 9 hours.

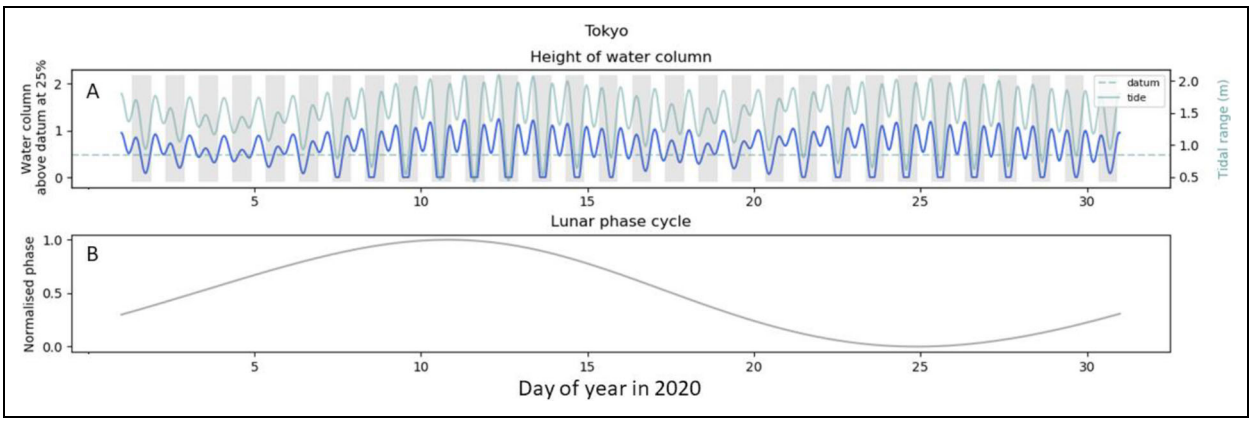

Figure 2. Modelled tidal cycle for Tokyo in January 2020. (A) Tidal cycle modelled for Tokyo for the period of January 1–31, 2020. Dark blue line is the height of the water column above the intertidal point; light blue line, the tidal range. (B) Lunar phase cycle, where 0 is new moon and 1 is full. Times (start of day) on x-axis are in GMT: Tokyo is GMT + 9 hours.

fixed to the day-night solar cycle. For the calculations shown in **Figure 2**, an intertidal point has been defined as 25% of the tidal range above the minimum tide (Tokyo: minimum tide = 0.80 m; maximum tide = 1.81 m; intertidal point = 1.05 m; maximum depth = 0.76 m), which mimics wetting and drying, as well as resulting in a variable-depth water column above that position.

The resulting changes to the shape (particularly the ALAN and solar signal) and the spectral composition of the intertidal irradiances for Tokyo are shown clearly in **Figure 3**. The ALAN time series no longer resembles a monotonous set of top-hat functions, but rather is modulated and differentially attenuated spectrally depending upon the state of the tide (depth of the water column), which itself occurs later on successive days throughout the night-time hours. The spectral irradiance values of ALAN for Tokyo $E(\lambda_{r,\ g,\ b})$ were 35.4, 35.5 and 66.1 μW m^{-2}, respectively, with corresponding values of the spectral diffuse attenuation coefficient $k_d(\lambda_{r,\ g,\ b})$ being 0.88, 0.56 and 1.13 m^{-1}, respectively (January climatological average). Despite $E(\lambda_b)$ being almost a factor of two greater than $E(\lambda_{r,\ g})$, the higher value of $k_d(\lambda_b)$ drives a more rapid attenuation with depth (Equation 3), which is amplified logarithmically when high tides occur during the hours of darkness, as shown on day 4 in **Figure 3C**. Conversely, during night-time low tides, the intertidal point is subjected to in-air levels of ALAN, as shown around day 11 in **Figure 3C**.

Downloaded from http://online.ucpress.edu/elementa/article-pdf/10/1/00042/765092/elementa.2022.00042.pdf by University of Strathclyde Glasgow user on 13 December 2022

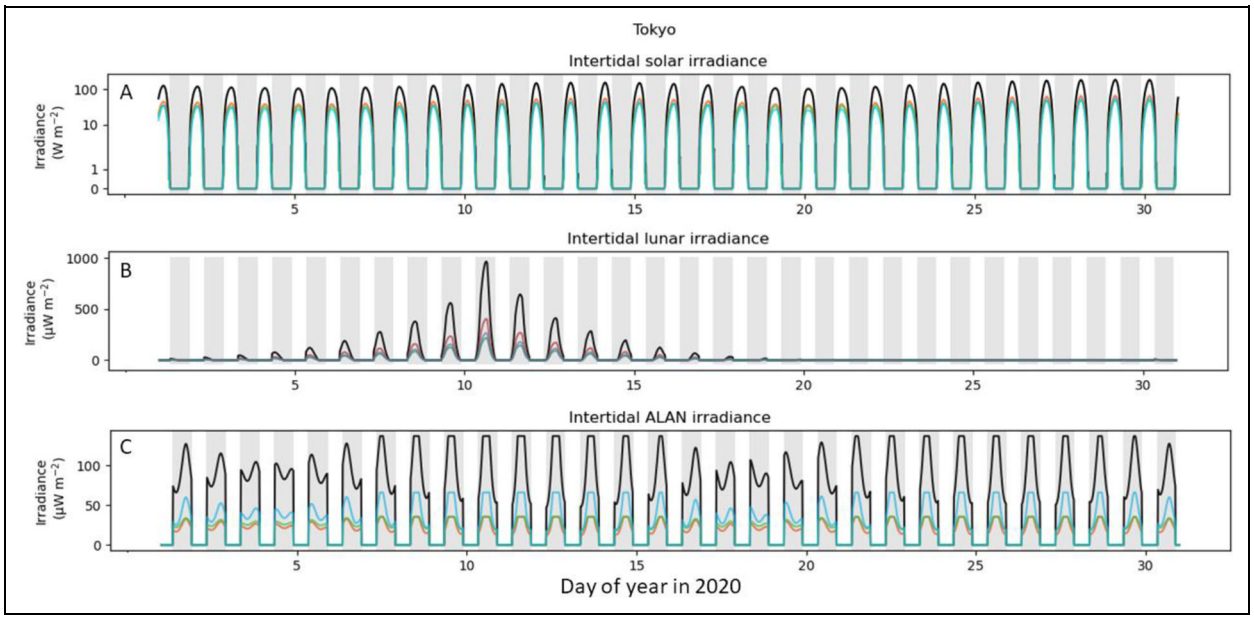

Figure 3. Impact of tides on sub-surface irradiances for Tokyo in January 2020. Spectral irradiances for (A) solar (blue), (B) lunar (green), and (C) artificial light at night (ALAN, red) and broadband (black) irradiances at the intertidal point calculated for Tokyo for the period January 1–31, 2020. Night-time periods are shown as grey bars. Times (start of day) on x-axis are in GMT: Tokyo is GMT + 9 hours.

The amount of exposure (dosage) to irradiances of differing spectral intensities, expressed in Joules per square meter (J m^{-2}), is a function of time and therefore integrative. The (monthly) dosage was calculated for each month by summing the modelled (15-minute timestep) instantaneous irradiances (W m^{-2} equivalent to J s^{-1} m^{-2}) over the time period(s) when a particular source is active. The solar and ALAN surface dosages are constrained by the length of day and night, respectively, which is a function of latitude and season. The lunar dosages are additionally constrained by phase and the position of the moon above the horizon during the night. **Figure 4** encapsulates all of these factors for the city of Shanghai (mid-latitude): solar monthly dosages are higher in the summer (400 MJ m^{-2}) compared with the winter (200 MJ m^{-2}); twilight monthly dosages remain relatively stable throughout the year at around 200 kJ m^{-2}, although a modelled time step of 15 minutes may not be sufficient to capture the variability, particularly in the period within an hour of sunset/sunrise; lunar monthly dosages reach a peak in the winter (200 J m^{-2}) and a minimum in the summer (<100 J m^{-2}), due to longer nights and higher full moon altitude angles during the winter; and ALAN monthly dosages unsurprisingly peak in the winter (at approximately 400 J m^{-2}) and reach a minimum in the summer (approximately 200 J m^{-2}), driven primarily by longer nights in the winter. Note that the solar dosages (MJ m^{-2}) are three orders of magnitude greater than twilight (kJ m^{-2}), which in turn are three orders of magnitude greater than lunar and ALAN dosages (J m^{-2}); modelled ALAN is approximately a factor of two greater than modelled lunar dosage for Shanghai. For all other cities studied, see Figures S1–S7.

Incorporation of the modelled tidal cycle at Shanghai (**Figure 5**) unsurprisingly lessens the monthly averaged dosage at this intertidal point, by a factor of between three and four. This decrease is governed primarily by the spectral value of k_d, which in turn also has monthly variability. For Shanghai, at the mouth of the Yangtze estuary, the annual average values of $k_d(\lambda_{r,\,g,\,b})$ used in our modelling ($n = 12$) are 1.20 ± 0.12 m^{-1}, 0.89 ± 0.18 m^{-1} and 1.69 ± 0.48 m^{-1}, respectively. These values are consistent with highly turbid waters containing a large amount of coloured dissolved organic matter, and correspond qualitatively with the spectral shapes reported by Yu (2019). The relatively large tidal range at Shanghai (modelled here as 3.4 m) coupled with these high in-water attenuations will further diminish the in-water dosage (from all sources) at the intertidal point. For the other cities studied, see Figures S8–S14.

Ranking each of the cities by seasonal surface ALAN dosage (**Figure 6**) shows little variability in the top 5 cities (range in parentheses): Los Angeles (335–467 J m^{-2}), New York (277–428 J m^{-2}), Buenos Aires (369–527 J m^{-2}), Shanghai (258–343 J m^{-2}) and Mumbai (223–260 J m^{-2}). The variability in ALAN dosage with season is driven by the change in daylength and explains why southern hemisphere Buenos Aires is the only megacity that has its peak in austral winter (JJA). The difference between ALAN and lunar dosage (range in parentheses) is: Los Angeles (271–290 J m^{-2}), New York (230–253 J m^{-2}), Buenos Aires (292–384 J m^{-2}), Shanghai (161–186 J m^{-2}) and Mumbai (79–121 J m^{-2}). The ALAN dosage can be almost a factor of six greater than lunar in some seasons (New York; see **Figure 6C**). By contrast, ALAN dosage in Lagos is comparable to lunar dosage (factor of 1–1.4). Lagos shows only

Downloaded from http://online.ucpress.edu/elementa/article-pdf/10/1/00042/765092/elementa.2022.00042.pdf by University of Strathclyde Glasgow user on 13 December 2022

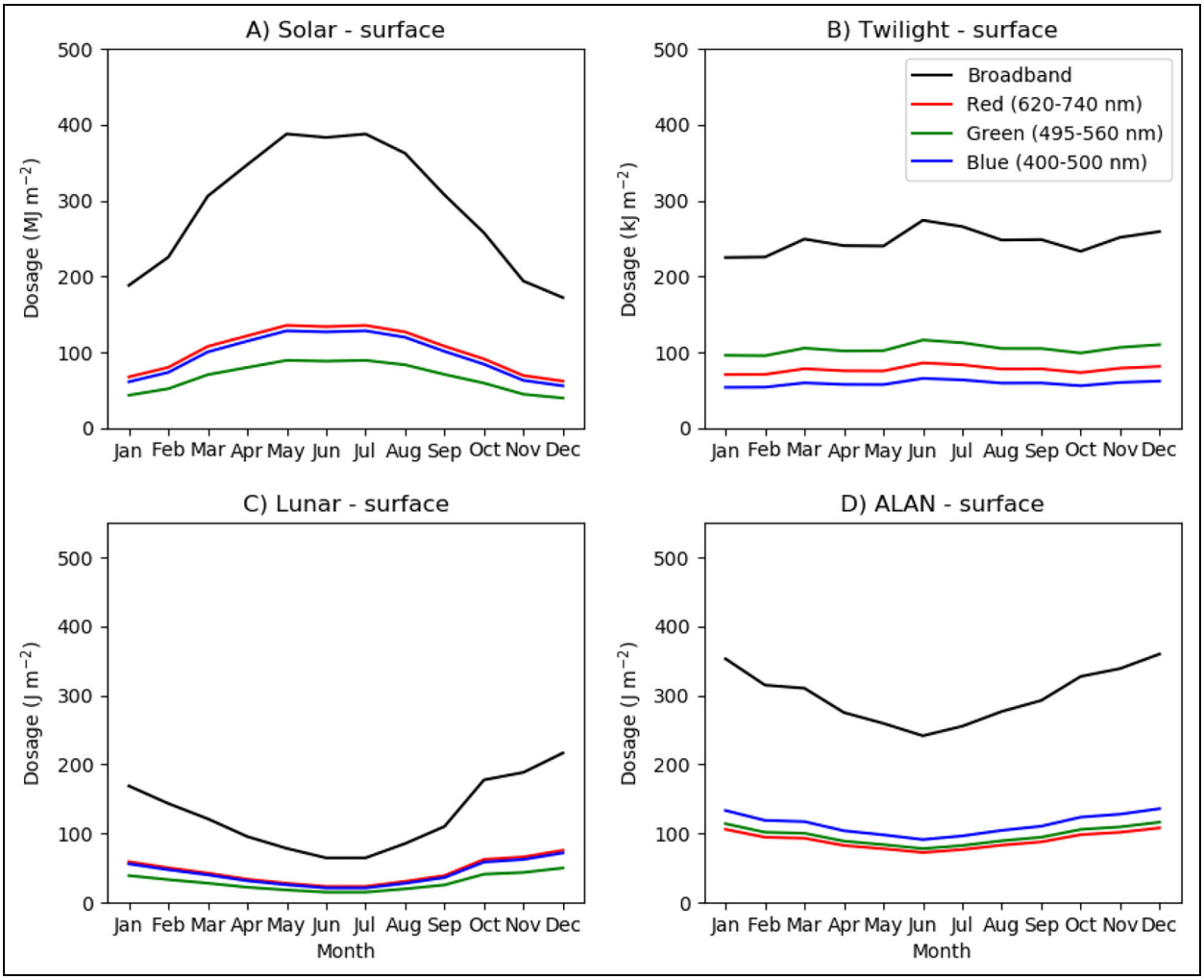

Figure 4. Monthly integrated dosages of irradiance at the surface calculated for Shanghai (2020). Model results for dosages of (A) solar (MJ m^{-2}), (B) twilight (kJ m^{-2}), (C) lunar (J m^{-2}), and (D) artificial light at night (ALAN, J m^{-2}); note the different units. Broadband (400–740 nm) is shown in black; spectral components, in blue (400–500 nm), green (495–560 nm), and red (620–740 nm).

a small amount of seasonal variability in lunar dosage and daylength due to its low latitude.

The combined effect of a realistic tidal signal and water clarity over different seasons is shown in **Figure 7**. The differences between ALAN and lunar dosages are most marked for Shanghai (typical rank drops from 4th to 8th) and Mumbai (typical rank drops from 5th to 7th). Shanghai is impacted by a relatively large tidal range and turbid water (as outlined above for **Figure 5**), as is Mumbai (tidal range: 2.8 m; annual average $k_d(\lambda_{r,\,g,\,b})$ values (n = 12) 1.09 ± 0.20 m^{-1}, 0.91 ± 0.46 m^{-1} and 1.94 ± 1.28 m^{-1} respectively). The megacities can be ranked by their seasonal mean maximum ALAN irradiance at the surface (**Figure 8**) and the intertidal point (**Figure 9**). The irradiance of the full moon always exceeds that of the ALAN irradiance in all of the cities studied (apart from Shanghai; see JJA in **Figure 9C**), although the ALAN dosage is generally higher. The impact of the tidal signal, coupled with the spectral clarity of the water column, can be seen in the modulation of the irradiances when comparing **Figures 8** and **9**; cities with a higher tidal range and more opaque waters (such as Shanghai and Mumbai; **Figure 9**) have a stronger in-water attenuation of the maximum lunar irradiance. In these cities the difference between the maximum ALAN and lunar irradiances is minimized. The variability in the natural rhythms of the lunar cycle with phase and season stands in marked contrast to the uniformity of ALAN (**Figure 1C**).

Variability over the 20-year period 2001–2020 for the city of Plymouth is shown in **Table 1** (mid-latitude location of 50.37°N). The lunar irradiance varies considerably: the integrated dosage ranges between 20 (June) and 170 (December) J m^{-2} and shows around ±25% interannual monthly variability at the surface; ALAN dosage is higher and considerably more uniform over that period, ranging between 98 (June) and 240 (December) J m^{-2}, with less than ±1% interannual monthly variability. Any month-on-month changes are due to the length of the night-time period. These patterns are repeated for the intertidal point data, with a reduction in the overall dosages and a slight increase in the amount of interannual monthly variability, particularly for the ALAN signal.

The spectral signature of ALAN is shifted towards the blue, both at the surface (**Table 2**) and at the intertidal

Downloaded from http://online.ucpress.edu/elementa/article-pdf/10/1/00042/765092/elementa.2022.00042.pdf by University of Strathclyde Glasgow user on 13 December 2022

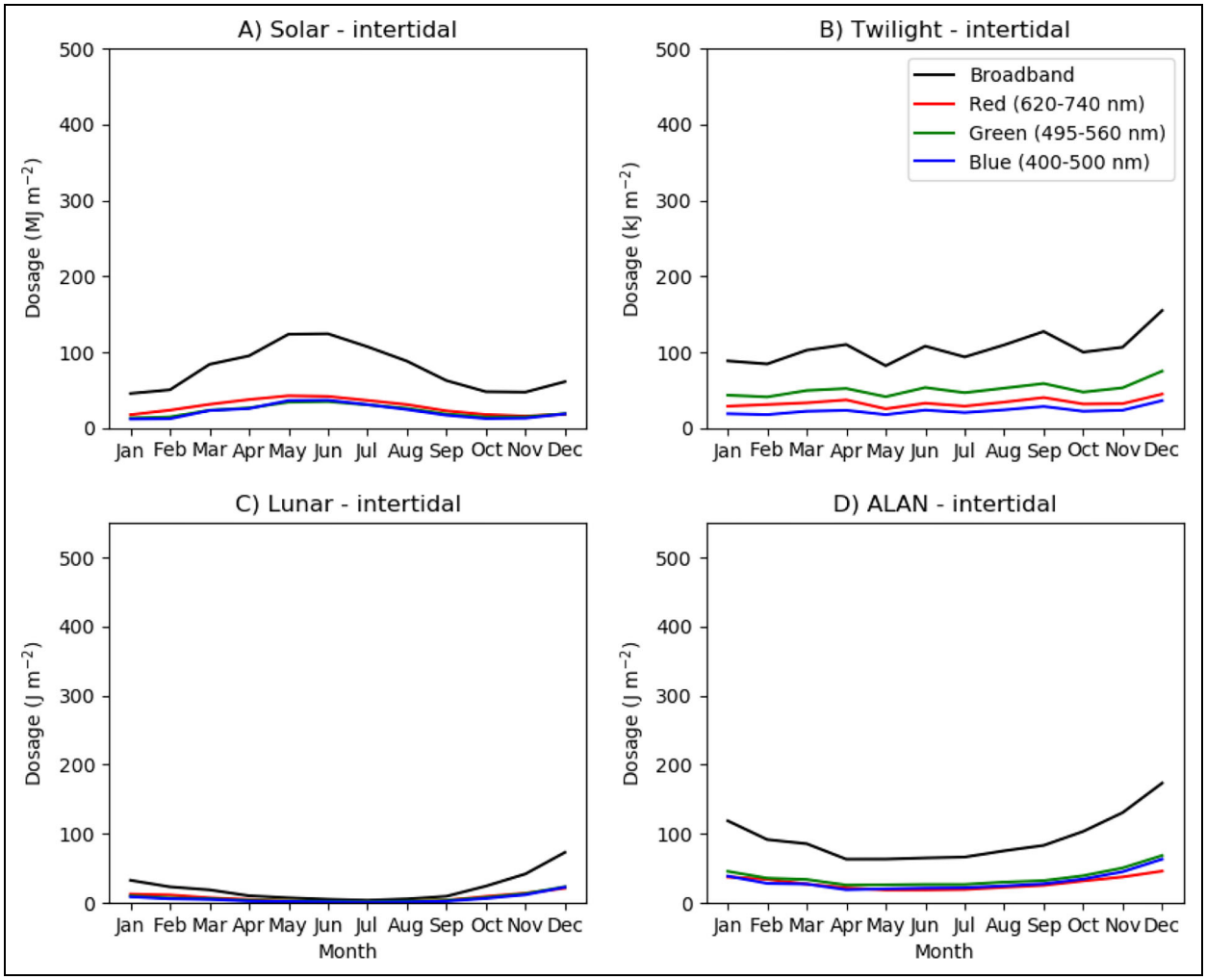

Figure 5. Monthly integrated dosages of irradiance at the intertidal point calculated for Shanghai (2020). Model results for dosages of (A) solar (MJ m^{-2}), (B) twilight (kJ m^{-2}), (C) lunar (J m^{-2}), and (D) artificial light at night (ALAN, J m^{-2}); note the different units. Broadband (400–740 nm) is shown in black; spectral components, in blue (400–500 nm), green (495–560 nm), and red (620–740 nm).

point (**Table 3**) for each megacity. At the surface, the ratio of blue to red light is typically between 1.06 (Buenos Aires) and 1.87 (Tokyo) for ALAN; and for the intertidal point, between 1.05 (Buenos Aires) and 2.60 (Plymouth). The intertidal point data also take into consideration the optical quality of the coastal water for each city; estuaries and coastal areas which are lower in coloured dissolved organic matter will allow a greater penetration of blue wavelength light, whereas absorption in the red is strongly determined by relatively invariant pure water absorption. For the natural lunar dosage, the ratio of blue to red is closer to 0.93 at the surface, with greater variability and variation between cities for the intertidal calculation, which ranges from 0.71 (Mumbai) to 1.20 (Plymouth).

Discussion

Implications

Our model incorporates realistic lunar and tidal components with spectrally resolved in-water attenuation coefficients. This advance makes it the first to quantify the relative intensities of spectral moonlight and ALAN in marine ecosystems near megacities.

The spectral quality of ALAN arriving at the intertidal point may further disrupt an array of visually guided ecological processes. Recent work by McMahon et al. (2022) demonstrated that broad spectrum lighting decreases the efficacy of camouflage at night in nature. Such interference with prey defense can potentially alter selective predation, population dynamics and the genetic structure of polymorphic populations. The precise spectral light intensities for a given location and position on the shoreline will be a function of the depth of the water column and the in-water diffuse attenuation coefficients, $k_d(\lambda)$, which change continuously with tides and seasons. Therefore, changes in predation pressure may be observed, impacting predator and prey species dynamics, particularly as ALAN differs substantially both spectrally and in its lack of a monthly cycle at the surface, being modulated somewhat at depth by the tidal cycle in terms of intensity and spectral signature.

The results of our modelling study show that ALAN dosage (i.e., total amount of light received) exceeds that of the natural night-time lunar source above and below the surface of the sea, across all seasons, and in all of the

Downloaded from http://online.ucpress.edu/elementa/article-pdf/10/1/00042/765092/elementa.2022.00042.pdf by University of Strathclyde Glasgow user on 13 December 2022

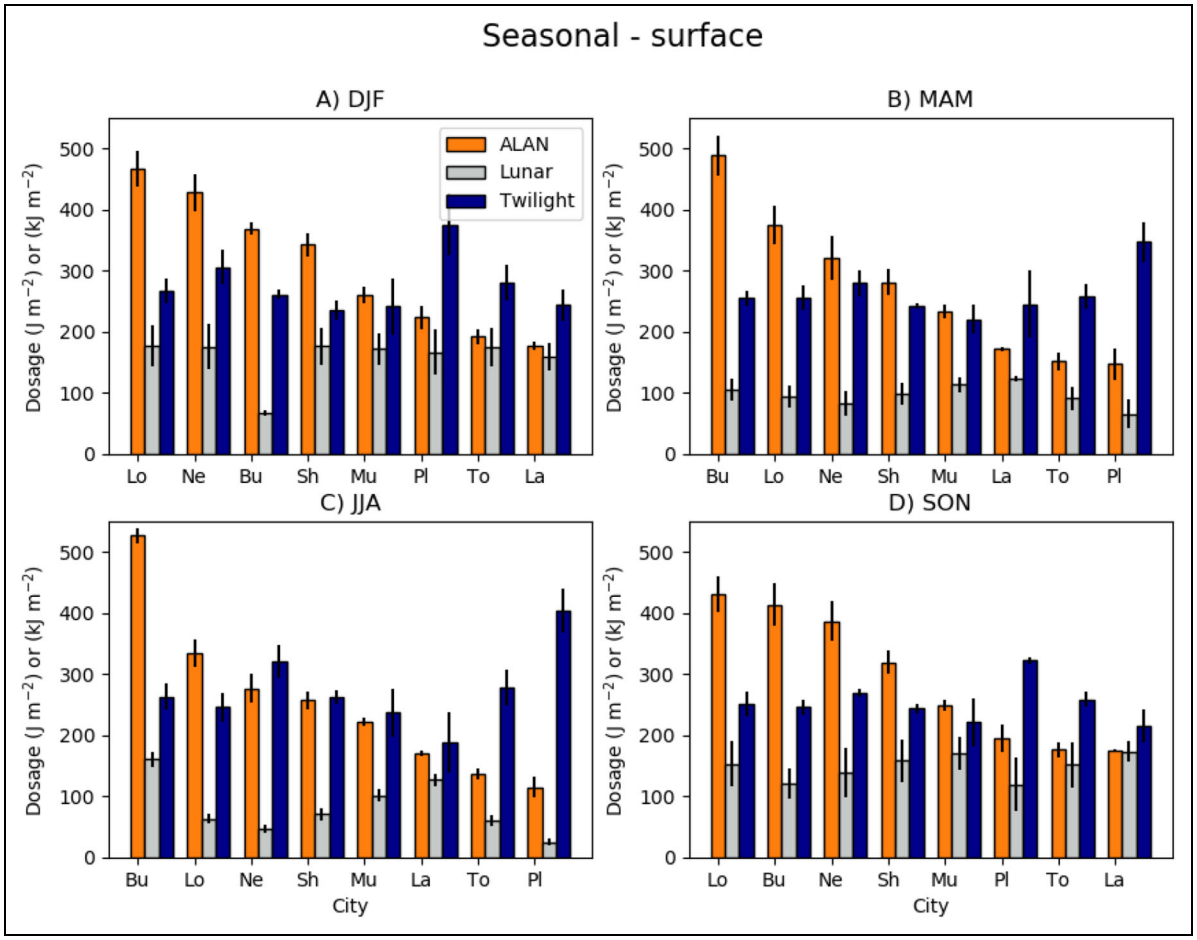

Figure 6. Cities ranked by mean seasonal dosages of artificial light at night (ALAN) at the surface. Irradiance dosages for (A) boreal winter (DJF), (B) boreal spring (MAM), (C) boreal summer (JJA), and (D) boreal autumn (SON) for ALAN (orange, J m^{-2}) compared to lunar (silver, J m^{-2}) and twilight (navy blue, kJ m^{-2}). Note the different dosage units for twilight (kJ m^{-2}) compared to ALAN and Lunar (J m^{-2}) in each panel. Cities are Los Angeles (Lo), New York (Ne), Buenos Aires (Bu), Shanghai (Sh), Mumbai (Mu), Plymouth (Pl), Tokyo (To), and Lagos (La). Error bars indicate standard deviation of the mean (n = 3).

metropolitan areas examined. This excess can be up to a factor of six greater (New York). However, when the moon reaches its maximum irradiance, which itself is a function of season and latitude, the lunar value exceeds that of ALAN. At midnight (zenith) on a full moon, the natural source outshines the anthropogenic by greater than a factor of ten (Lagos). Although the maximum lunar irradiance will likely still be experienced at these locations, ALAN will drive the total irradiance received over the course of the night. Throughout the passage of the night, the changing pathlength of light through the atmosphere will act to diminish the lunar signal, whereas the anthropogenic sources will remain constant during that period. The de facto absence of a seasonal lunar signal detectable by organisms could have many adverse effects given how widespread lunar-guided phenological processes are in nature (Naylor, 2001; Boch et al., 2011; Kronfeld-Schor et al., 2013; Last et al., 2016; Righton et al., 2016; Ugolini et al., 2016; Ludvigsen et al., 2018; Torres et al., 2020).

The lunar brightening around the time of the full moon, known as lunar opposition (**Figure 1B**), is the dominant factor in the maximum lunar irradiance experienced (**Figure 8**). There is a sharp reduction in the lunar irradiance with increasing atmospheric pathlength, and at times away from the full moon. Therefore, between new moon and the first quarter in the waxing phase, and from last quarter to new in the waning, ALAN is likely to be the dominant source of light at night for all cities. Many marine species, such as oysters (Payton and Tran, 2019), time their activity around the darker nights of the lunar cycle and could be adversely affected by constant illumination.

Natural skyscapes in remote terrestrial (such as Arctic tundra, Antarctica, forests) or marine (far offshore, >100 km) locations, distant from anthropogenic activities and settlements, are never truly dark, even on moonless nights. In these locations, the combination of starlight, diffuse galactic light (scattering by interstellar dust grains), airglow (emission from atoms and molecules in the Earth's upper atmosphere) and zodiacal light (sunlight scattered by dust in the solar system) all contribute to the natural sky brightness. These sources vary over season, geographical location and solar cycle, interacting in a largely unpredictable manner. These natural skyscapes on moonless

Downloaded from http://online.ucpress.edu/elementa/article-pdf/10/1/00042/765092/elementa.2022.00042.pdf by University of Strathclyde Glasgow user on 13 December 2022

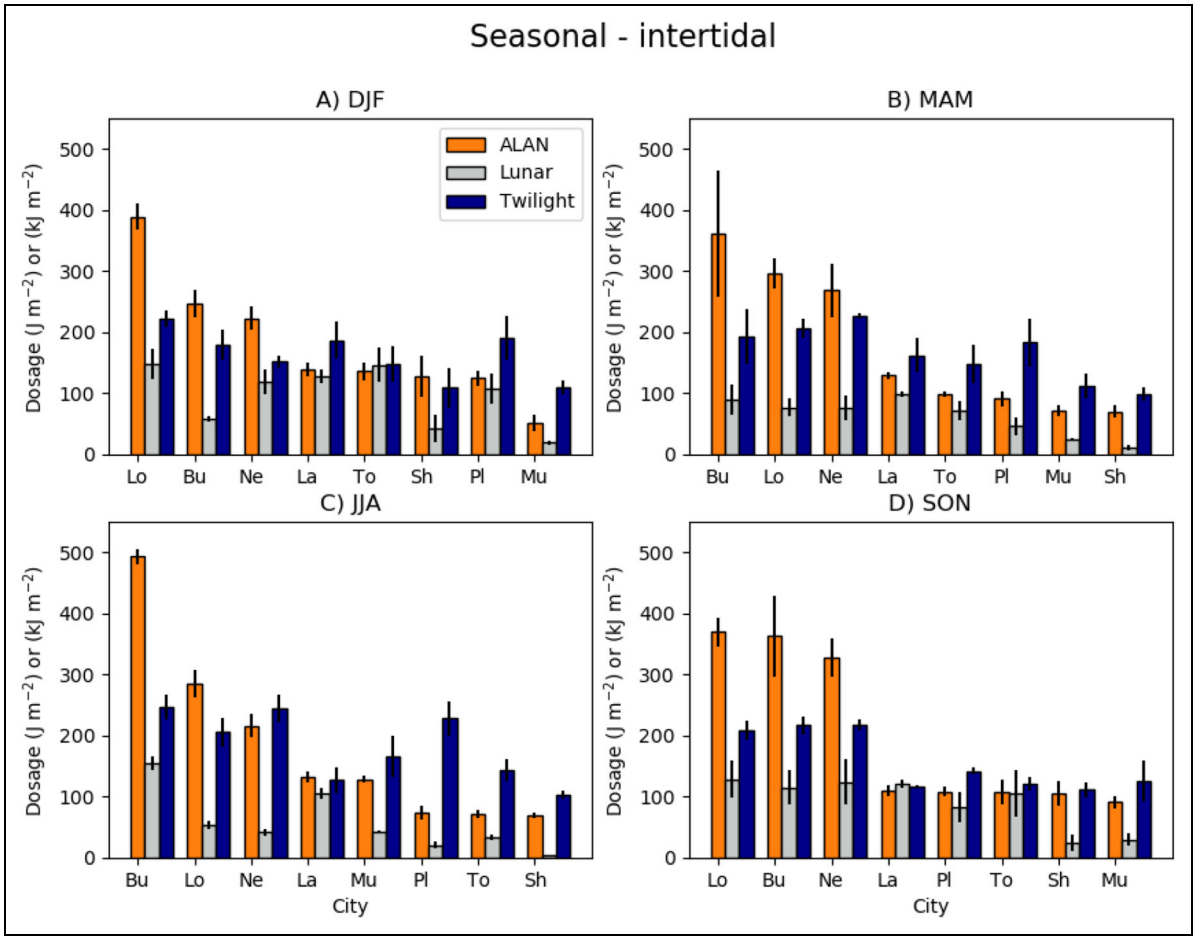

Figure 7. Cities ranked by mean seasonal dosages of artificial light at night (ALAN) at intertidal point. Irradiance dosages for (A) boreal winter (DJF), (B) boreal spring (MAM), (C) boreal summer (JJA), and (D) boreal autumn (SON) for ALAN (orange, J m^{-2}) compared to lunar (silver, J m^{-2}) and twilight (navy blue, kJ m^{-2}). Cities are Los Angeles (Lo), New York (Ne), Buenos Aires (Bu), Shanghai (Sh), Mumbai (Mu), Plymouth (Pl), Tokyo (To), and Lagos (La). Note the different dosage units for twilight (kJ m^{-2}) compared to ALAN and Lunar (J m^{-2}) in each panel. Error bars indicate standard deviation of the mean (n = 3).

nights have a brightness of around 22 mag arcsecond^{-2} (Alarcon et al., 2021) which is approximately 0.25 μW m^{-2}; comparing this value with **Figure 8** shows that the typical range of ALAN levels for the megacities studied is 100–400 μW m^{-2} and for lunar, 200–1200 μW m^{-2}. The natural skyscape brightness is of the same order of magnitude as the minimum irradiance of white light (approximately 0.1 μW m^{-2}) that elicits diel vertical migration in globally widespread adult *Calanus* copepods (Båtnes et al., 2015).

Marine ecosystems are particularly likely to be affected in the most heavily light-polluted megacities (Los Angeles, New York, Buenos Aires, Shanghai, Mumbai). The greatest direct impacts are on highly photosensitive species that utilize moonlight to guide migrations and synchronize phenological events (Naylor, 2001; Last et al., 2016; Ugolini et al., 2016; Ludvigsen et al., 2018; Torres et al., 2020), many of which are critical to the wider ecosystem, such as coral reefs, and sustain vital ecosystem services (Moberg and Folke, 1999; Hayes, 2003). The near-field effects of individual street lights, although considerable on scales <10 m, rapidly decrease with distance, and when interacting with the aquatic environment, much of the light is reflected at the surface (Jechow and Hölker, 2019). It is the far-field skyglow that will tend to dominate the in-water impacts at distances >100 m, as point sources appear closer to the horizon.

Our modeling also predicts that coastal water clarity, $k_d(\lambda)$, in combination with tidal dynamics will determine the propagation of spectral light from all sources, natural and anthropogenic, to benthic habitats. Recent work (Davies et al., 2020) demonstrated that differential spectral attenuation determines the extent to which coastal benthic habitats are exposed to ALAN; that is, the areal extent of the ALAN footprint. Here we have demonstrated that tidal dynamics play a substantial role in modulating the exposure of benthic habitats to ALAN. A promising area for research could be to quantify the response of animals to ALAN over the spring/neap cycle. Our analysis of megacities shows that the intensity of surface ALAN irradiance combined with the local-scale water clarity will determine the total footprint of ALAN exposure. More opaque coastal waters (either through natural sources or anthropogenic pollution) reduce the total footprint of

Downloaded from http://online.ucpress.edu/elementa/article-pdf/10/1/00042/765092/elementa.2022.00042.pdf by University of Strathclyde Glasgow user on 13 December 2022

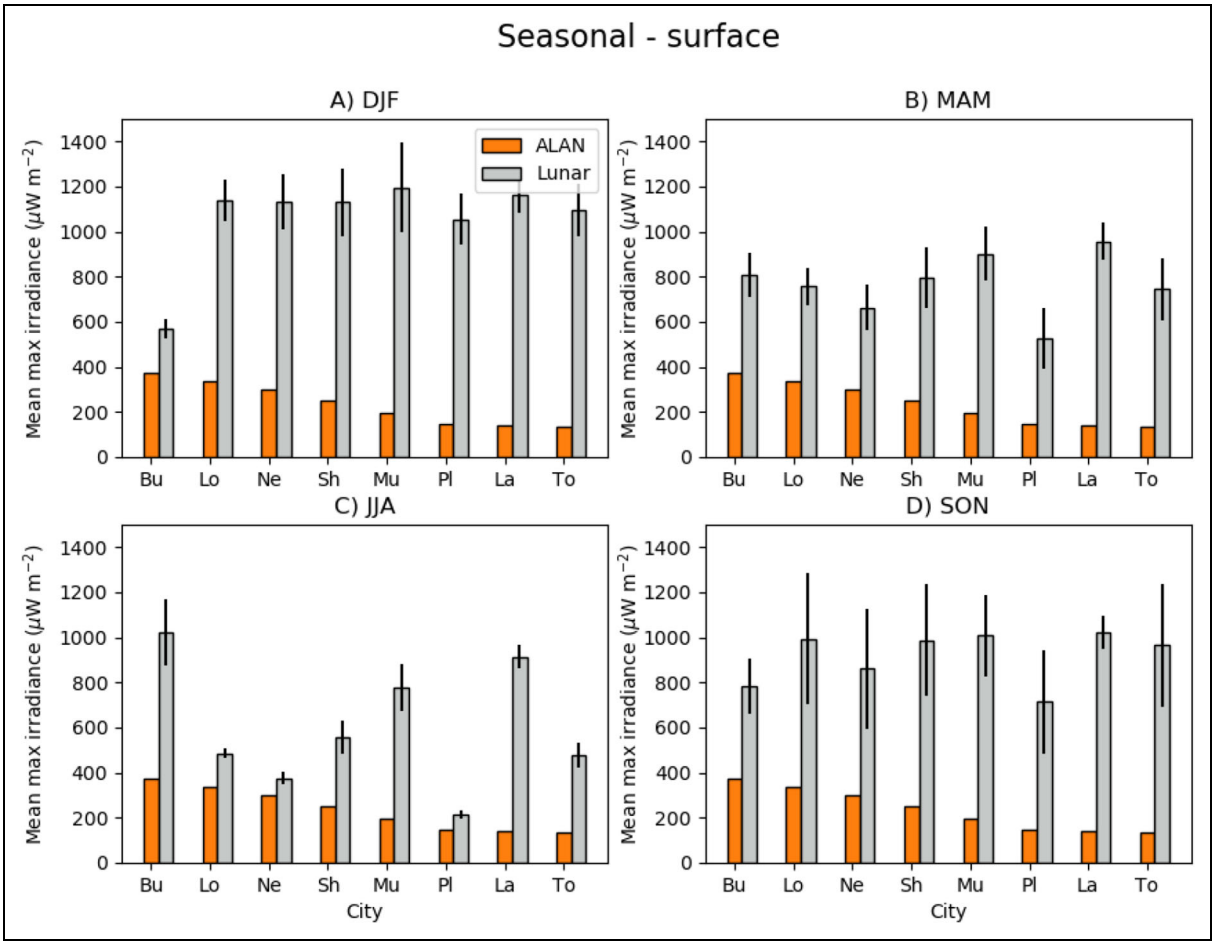

Figure 8. Cities ranked by mean seasonal maximum irradiance for artificial light at night (ALAN) at the surface. Maximum irradiances for (A) boreal winter (DJF), (B) boreal spring (MAM), (C) boreal summer (JJA), and (D) boreal autumn (SON) for ALAN (orange, μW m^{-2}) compared to lunar (silver, μW m^{-2}). Cities are Los Angeles (Lo), New York (Ne), Buenos Aires (Bu), Shanghai (Sh), Mumbai (Mu), Plymouth (Pl), Tokyo (To), and Lagos (La). Error bars indicate standard deviation of the mean (n = 3).

ALAN experienced in benthic habitats. Whilst the trade-offs between two types of anthropogenic pollution (i.e., coastal water pollution and ALAN) may be difficult to manage, this reduction does raise the question of whether seabed species that provide shading of the seabed (Gerard, 1984) may be used as a nature-based solution to combat ALAN along heavily lit coasts, much in the same way that amelioration of thermal heat and biodiversity can be promoted by this solution (Bulleri et al., 2018). Indeed, seaweed can form canopies several meters deep at high tide, but shading from these species to ameliorate the impacts of ALAN, especially in heavily lit coastal areas, is unknown. This potential solution, however, will also need to be balanced against the fundamental way in which seaweed will impact natural light penetration during both daylight and night-time hours and the likely conflict of large swaths of seaweed beds in urban areas with aesthetic and tourism values.

Limitations of approach

The relationship between artificial sky brightness and sea-surface spectral irradiance was derived from measurements of artificial skyglow originating from the city of Plymouth, UK, recorded on clear moonless nights when the sun was >18° below the horizon. Whilst the derived relationships are robust (Davies et al., 2020; Smyth et al., 2021), our modelling approach assumes that the spectral power distribution of artificial skyglow is matched between Plymouth, a predominantly LED-lit city, and the megacities investigated here. While LED lighting use is growing rapidly and forecast to contribute 97% of the global lighting market by 2025 (Bertoldi, 2018), the modelled exposure levels may overestimate artificial light irradiances where LPS lighting is still in use; however, these levels will remain broadly representative where other modern broad-spectrum lights (e.g., high pressure sodium and metal halide) predominate.

Our modelling assumed clear sky conditions for a given megacity. In reality cloud cover will vary in time and space. The impacts of clouds on the night-time skyscape are twofold: firstly, to block any incoming lunar or twilight irradiance, partially or completely; and secondly to amplify the near-field impacts of ALAN (Kyba et al., 2011; Jechow et al., 2017). Both impacts are difficult to quantify as both will be a function of cloudiness, which is highly subjective as the radiative properties of clouds vary

Downloaded from http://online.ucpress.edu/elementa/article-pdf/10/1/00042/765092/elementa.2022.00042.pdf by University of Strathclyde Glasgow user on 13 December 2022

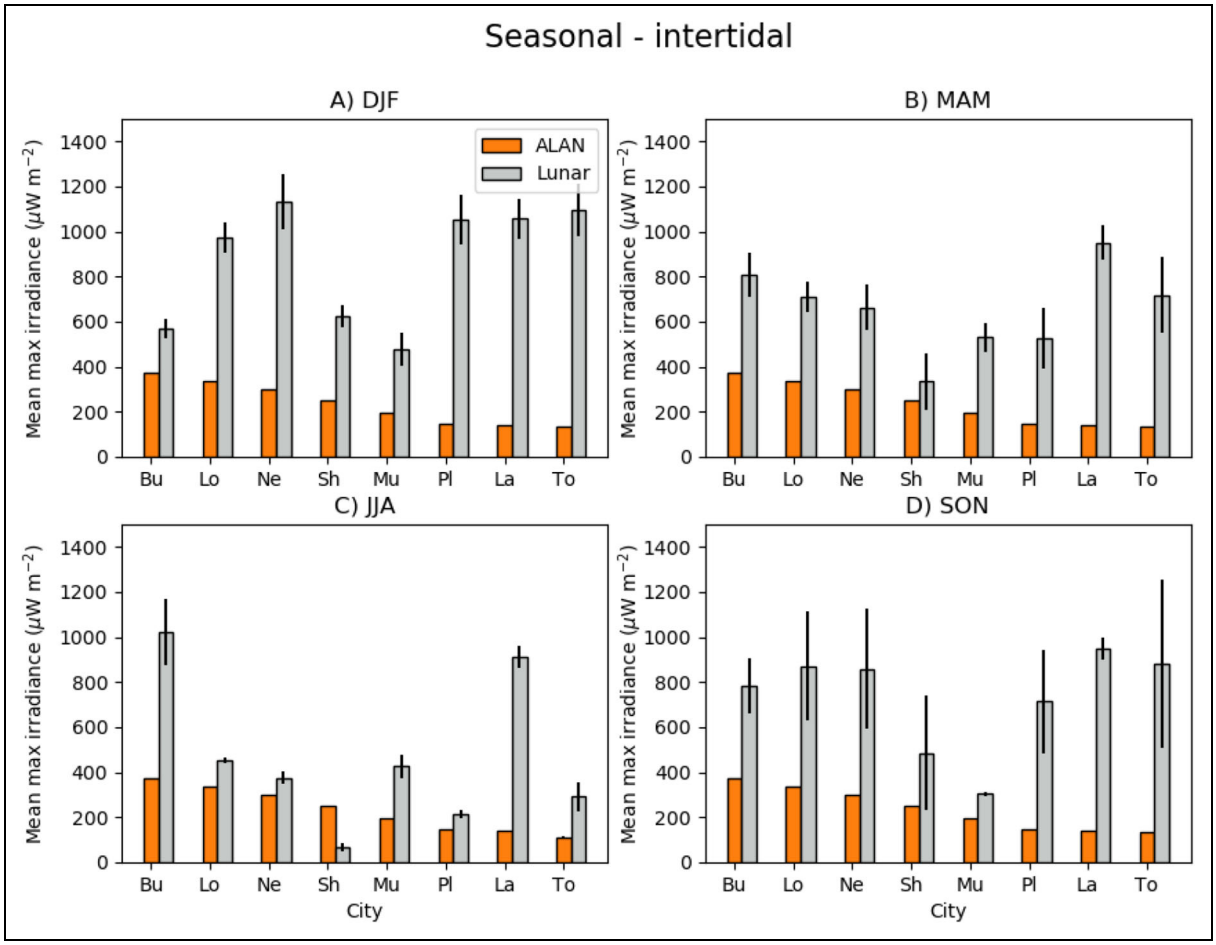

Figure 9. Cities ranked by mean seasonal maximum irradiance for artificial light at night (ALAN) at intertidal point. Maximum irradiances for (A) boreal winter (DJF), (B) boreal spring (MAM), (C) boreal summer (JJA), and (D) boreal autumn (SON) for ALAN (orange, μW m^{-2}) compared to lunar (silver, μW m^{-2}). Cities are Los Angeles (Lo), New York (Ne), Buenos Aires (Bu), Shanghai (Sh), Mumbai (Mu), Plymouth (Pl), Tokyo (To), and Lagos (La). Error bars indicate standard deviation of the mean (n = 3).

Table 1. Mean monthly dosage and associated standard deviation (n = 20) for lunar irradiance and artificial light at night (ALAN) at the surface and intertidal point in the water column over a 20-year time period for the city of Plymouth (2001–2020)

Month	Surface Lunar Dosage (J m^{-2})	Surface ALAN Dosage (J m^{-2})	Intertidal Lunar Dosage (J m^{-2})	Intertidal ALAN Dosage (J m^{-2})
Jan	159.95 ± 17.26	233.29 ± 0.15	101.52 ± 10.11	125.99 ± 2.67
Feb	118.78 ± 17.08	191.93 ± 2.80	79.54 ± 10.92	109.58 ± 2.71
Mar	92.99 ± 16.32	180.80 ± 0.26	65.90 ± 11.09	109.23 ± 1.88
Apr	54.95 ± 10.38	143.84 ± 0.27	40.44 ± 7.42	89.54 ± 1.47
May	31.89 ± 7.70	118.19 ± 0.31	25.45 ± 6.08	80.64 ± 1.03
Jun	20.36 ± 5.32	97.55 ± 0.06	16.53 ± 4.31	63.64 ± 0.80
Jul	25.35 ± 6.25	109.91 ± 0.32	21.21 ± 5.14	71.51 ± 0.99
Aug	45.13 ± 9.52	137.33 ± 0.36	36.80 ± 7.31	88.60 ± 1.47
Sep	74.30 ± 11.70	163.81 ± 0.34	55.94 ± 7.95	98.12 ± 1.94
Oct	115.74 ± 18.11	200.50 ± 0.33	81.06 ± 12.09	113.77 ± 2.21
Nov	159.95 ± 17.26	233.29 ± 0.15	101.52 ± 10.11	125.99 ± 2.67
Dec	171.25 ± 22.19	240.59 ± 0.07	116.05 ± 14.05	142.72 ± 2.34

Downloaded from http://online.ucpress.edu/elementa/article-pdf/10/1/00042/765092/elementa.2022.00042.pdf by University of Strathclyde Glasgow user on 13 December 2022

Table 2. Annual dosage (2020) of irradiance at the surface, assuming clear skies, from the primary source terms of solar, lunar, artificial light at night (ALAN) and twilight, where G, M, and k indicate $\times$ 10^9, 10^6, and 10^3, respectively

		Broad Wavelength Bands		
City	**Source**	**Red (J m^{-2})**	**Green (J m^{-2})**	**Blue (J m^{-2})**
Buenos Aires	Solar	1.210 G	791 M	1.130 G
	Lunar	0.481 k	0.314 k	0.448 k
	ALAN	1.710 k	1.880 k	1.810 k
	Twilight	967 k	1.300 M	736 k
Lagos	Solar	1.460 G	960 M	1.380 G
	Lunar	0.610 k	0.402 k	0.578 k
	ALAN	0.545 k	0.552 k	0.988 k
	Twilight	841 k	1.130 M	641 k
Los Angeles	Solar	1.200 G	782 M	1.120 G
	Lunar	0.515 k	0.337 k	0.481 k
	ALAN	1.510 k	1.650 k	1.660 k
	Twilight	962 k	1.300 M	733 k
Mumbai	Solar	1.380 G	906 M	1.300 G
	Lunar	0.586 k	0.386 k	0.553 k
	ALAN	0.831 k	0.878 k	1.190 k
	Twilight	867 k	1.170 M	661 k
New York	Solar	1.090 G	710 M	1.010 G
	Lunar	0.472 k	0.307 k	0.438 k
	ALAN	1.310 k	1.420 k	1.510 k
	Twilight	1.110 M	1.490 M	843 k
Plymouth	Solar	918 M	594 M	843 M
	Lunar	0.402 k	0.261 k	0.371 k
	ALAN	0.540 k	0.550 k	0.951 k
	Twilight	1.370 M	1.840 M	1.040 M
Shanghai	Solar	1.240 G	810 M	1.160 G
	Lunar	0.532 k	0.349 k	0.498 k
	ALAN	1.080 k	1.160 k	1.360 k
	Twilight	929 k	1.250 M	708 k
Tokyo	Solar	1.170 G	766 M	1.090 G
	Lunar	0.507 k	0.331 kJ	0.473 k
	ALAN	0.509 k	0.512 kJ	0.951 k
	Twilight	1.010 M	1.370 MJ	772 k

with type, height, thickness, layering and where they are distributed in the sky. However, cloud cover and cloud base have been shown to amplify ALAN pollution (Davies et al., 2020) by an order of magnitude in luminance (Kyba et al., 2011). Although research on biological responses to ALAN under different levels of cloud cover are few and inconclusive (Dwyer et al., 2013; Torres et al., 2020), it shows that animals detect seemingly subtle changes in intensity.

Whilst an indication of variability in the lunar signal over a 20-year period was calculated for Plymouth, it was not matched by the changes in the above-water ALAN, which would have been driven by a wholesale transition from LPS to LED in the period 2001–2020. Variability in the in-water $k_d(\lambda)$, which modulates the ALAN field through the water column, was captured on a climatological monthly basis, but extreme episodic events, such as high river discharges, would add significantly to the

Downloaded from http://online.ucpress.edu/elementa/article-pdf/10/1/00042/765092/elementa.2022.00042.pdf by University of Strathclyde Glasgow user on 13 December 2022

Table 3. Annual dosage (2020) of irradiance at the intertidal point, assuming clear skies, from the primary source terms of solar, lunar, artificial light at night (ALAN) and twilight, where G, M, and k indicate $\times$ 10^9, 10^6, and 10^3, respectively

		Broad Wavelength Bands		
City	**Source**	**Red (J m^{-2})**	**Green (J m^{-2})**	**Blue (J m^{-2})**
Buenos Aires	Solar	939 M	652 M	828 M
	Lunar	0.433 k	0.296 k	0.409 k
	ALAN	1.370 k	1.620 k	1.440 k
	Twilight	776 k	1.120 M	583 k
Lagos	Solar	1.080 G	791 M	962 M
	Lunar	0.475 k	0.340 k	0.420 k
	ALAN	0.399 k	0.450 k	0.672 k
	Twilight	555 k	863 k	385 k
Los Angeles	Solar	864 M	726 M	1.010 G
	Lunar	0.365 k	0.311 k	0.433 k
	ALAN	1.070 k	1.520 k	1.490 k
	Twilight	671 k	1.190 M	654 k
Mumbai	Solar	439 M	377 M	352 M
	Lunar	0.132 k	0.114 k	0.094 k
	ALAN	0.306 k	0.389 k	0.369 k
	Twilight	494 k	738 k	340 k
New York	Solar	799 M	608 M	793 M
	Lunar	0.379 k	0.265 k	0.348 k
	ALAN	0.919 k	1.150 k	1.090 k
	Twilight	750 k	1.190 M	596 k
Plymouth	Solar	440 M	468 M	588 M
	Lunar	0.226 k	0.211 k	0.271 k
	ALAN	0.238 k	0.415 k	0.618 k
	Twilight	472 k	1.310 M	616 k
Shanghai	Solar	336 M	270 M	263 M
	Lunar	0.090 k	0.081 k	0.069 k
	ALAN	0.340 k	0.441 k	0.371 k
	Twilight	401 k	615 k	279 k
Tokyo	Solar	790 M	590 M	658 M
	Lunar	0.376 k	0.272 k	0.326 k
	ALAN	0.320 k	0.376 k	0.521 k
	Twilight	528 k	893 k	331 k

variability in the signal. This added variability gives scope to further investigate regional differences, such as the impact that the seasonal monsoon might have on both ALAN exposure and biological light-guided processes in general.

Sky brightness data over each megacity was extracted from the Falchi et al. (2016) atlas that uses the Day Night Band (DNB) of the VIIRS satellite sensor, which is "blind" in the blue part of the spectrum and cannot distinguish spectrally between sodium-based lights and the longer wavelength component of the LED emission spectrum. The outputs of our methodology could therefore be improved by new satellite missions which could quantify spectrally the ALAN signature of individual megacities.

Conclusion

Our modelling study has shown that ALAN dominates the megacity night-time skyscape over all seasons, and that the natural illumination rhythms provided for millennia

Downloaded from http://online.ucpress.edu/elementa/article-pdf/10/1/00042/765092/elementa.2022.00042.pdf by University of Strathclyde Glasgow user on 13 December 2022

are disrupted for neighboring marine ecosystems. Only over the period close to the zenith full moon, and particularly at mid-latitude winter, does lunar irradiance outshine its anthropogenic competitor. Given the taxonomically widespread occurrence of animals that time crucial physiological, behavioral and life-history processes to changing lunar intensity, their marine ecosystems may already be facing fundamental disruptions. We show that the binary "on-off" pattern of ALAN, its intensity and spectral signature are considerably modulated by the ebb and flow of the tide as well as water clarity (IOPs). Quantifying ALAN in nature is challenging but warranted in order to facilitate a better understanding of the ecological exposure of animals and ecosystems and to provide biologists with guidance on future research on the impacts of ALAN.

Data accessibility statement

Code used to create the global megacity simulations can be accessed via https://github.com/timjsmyth/TidalLight.

Supplemental files

The supplemental files for this article can be found as follows:

- **Table S1.** Monthly values of spectral k_d (derived from the global IOP model via radiative transfer modelling; Smyth et al., 2021), spectral ALAN (derived from **Table 1** in Smyth et al., 2021), and sky brightness (Falchi et al., 2016) for each city (latitude and longitude given).
  - Filename: "ALAN_Kd_Falchi_MegaCities.xlsx"
- **Table S2.** Tidal data sets for each city used to determine the tidal harmonics allowing tides to be predicted for future dates.
  - Filename: "Tides_MegaCities.xlsx"
- **Figures S1–S14** showing the equivalent of **Figures 4** and **5** (Shanghai) for the megacities studied.
  - Filename: "Supplementary_figures_megacities_dosage_surface_intertidal.docx"

Acknowledgments

The authors would like to thank Fabio Falchi for making the entire floating-point dataset from the 2016 World Atlas of Artificial Night Sky Brightness available to us upon request. The authors would also like to thank Mike Bedington for advice on global tidal modeling and Jeff Conrad and Tom Shatwell for advice on lunar irradiance modeling.

Funding

This work was supported by UK Natural Environment Research Council grant NE/S003568/1 (TS, TD, DM, AW, ST, and AQ) and UK Natural Environment Research Council grant NE/X006271/1 (TS, OR, and AEJ).

Competing interests

The authors have declared that no competing interests exist.

Author contributions

Contributed to conception and design: TS, AW, TD.

Contributed to acquisition of data: TS, DM, TD.

Contributed to analysis and interpretation of data: TS, AW, DM, TD.

Drafted and/or revised this article: TS, AW, AEJ, DM, AQ, OR, ST, TD.

Approved the submitted version for publication: TS, AW, AEJ, DM, AQ, OR, ST, TD.

References

Alarcon, MR, **Serra-Ricart, M**, **Lemes-Perera, S**, **Mallorquín, M.** 2021. Natural night sky brightness during solar minimum. *The Astronomical Journal* **162**(1): 25. DOI: http://dx.doi.org/10.3847/1538-3881/abfdaa.

Ayalon, I, **Rosenberg, Y**, **Benichou, JIC**, **Campos, CLD**, **Sayco, SLG**, **Nada, MAL**, **Baquiran, JIP**, **Ligson, CA**, **Avisar, D**, **Conaco, C**, **Kuechly, HU**, **Kyba, CCM**, **Cabaitan, PC**, **Levy, O.** 2021. Coral gametogenesis collapse under artificial light pollution. *Current Biology* **31**(2): 413–419. DOI: http://dx.doi.org/10.1016/j.cub.2020.10.039.

Båtnes, AS, **Miljeteig, C**, **Berge, J**, **Greenacre, M**, **Johnsen, G.** 2015. Quantifying the light sensitivity of *Calanus* spp. during the polar night: Potential for orchestrated migrations conducted by ambient light from the sun, moon, or aurora borealis? *Polar Biology* **38**(1): 51–65. DOI: http://dx.doi.org/10.1007/s00300-013-1415-4.

Becker, A, **Whitfield, AK**, **Cowley, PD**, **Järnegren, J**, **Næsje, TF.** 2013. Potential effects of artificial light associated with anthropogenic infrastructure on the abundance and foraging behaviour of estuary-associated fishes. *Journal of Applied Ecology* **50**: 43–50. DOI: http://dx.doi.org/10.1111/1365-2664.12024.

Berge, J, **Geoffroy, M**, **Daase, M**, **Cottier, F**, **Priou, P**, **Cohen, JH**, **Johnsen, G**, **McKee, D**, **Kostakis, I**, **Renaud, PE**, **Vogedes, D**, **Anderson, P**, **Last, KS**, **Gauthier, S.** 2020. Artificial light during the polar night disrupts Arctic fish and zooplankton behaviour down to 200 m depth. *Communications Biology* **3**(1): 1–8. DOI: http://dx.doi.org/10.1038/s42003-020-0807-6.

Bertoldi, G. 2018. *Status of LED-lighting world market in 2017.* Ispra, Italy: European Commission.

Boch, CA, **Ananthasubramaniam, B**, **Sweeney, AM**, **Doyle, FJ**, **Morse, DE.** 2011. Effects of light dynamics on coral spawning synchrony. *Biological Bulletin* **220**(3): 161–173. DOI: http://dx.doi.org/10.1086/BBLv220n3p161.

Bulleri, F, **Eriksson, BK**, **Queiros, A**, **Airoldi, L**, **Arenas, F**, **Arvanitidis, C**, **Bouma, TJ**, **Crowe, TP**, **Davoult, D**, **Guizien, K**, **Ivesa, L**, **Jenkins, SR**, **Michalet, R**, **Olabarria, C**, **Procaccini, G**, **Serrao, EA**, **Wahl, M**, **Benedetti-Cecchi, L.** 2018. Harnessing positive species interactions as a tool against climate-driven loss of coastal biodiversity. *PLoS Biology* **16**(9): e2006852. DOI: http://dx.doi.org/10.1371/journal.pbio.2006852.

Downloaded from http://online.ucpress.edu/elementa/article-pdf/10/1/00042/765092/elementa.2022.00042.pdf by University of Strathclyde Glasgow user on 13 December 2022

Buratti, BJ, **Hiller, JK**, **Wang, M.** 1996. The lunar opposition surge: Observations by Clementine. *Icarus* **124**(2): 490–499. DOI: http://dx.doi.org/10.1006/icar.1996.0225.

Davies, TW, **Coleman, M**, **Griffith, KM**, **Jenkins, SR.** 2015. Night-time lighting alters the composition of marine epifaunal communities. *Biology Letters* **11**(4): 20150080. DOI: http://dx.doi.org/10.1098/rsbl.2015.0080.

Davies, TW, **Duffy, JP**, **Bennie, J**, **Gaston, KJ.** 2014. The nature, extent, and ecological implications of marine light pollution. *Frontiers in Ecology and the Environment* **12**(6): 347–355.

Davies, TW, **McKee, D**, **Fishwick, J**, **Tidau, S**, **Smyth, T.** 2020. Biologically important artificial light at night on the seafloor. *Scientific Reports* **10**(1): 12545. DOI: http://dx.doi.org/10.1038/s41598-020-69461-6.

Davies, TW, **Smyth, T.** 2018. Why artificial light at night should be a focus for global change research in the 21st century. *Global Change Biology* **24**(3): 872–882. DOI: http://dx.doi.org/10.1111/gcb.13927.

Diamantopoulou, C, **Christoforou, E**, **Dominoni, DM**, **Kaiserli, E**, **Czyzewski, J**, **Mirzai, N**, **Spatharis, S.** 2021. Wavelength-dependent effects of artificial light at night on phytoplankton growth and community structure. *Proceedings of the Royal Society B-Biological Sciences* **288**(1953): 20210525. DOI: http://dx.doi.org/10.1098/rspb.2021.0525.

Dierssen, HM, **Chlus, A**, **Russell, B.** 2015. Hyperspectral discrimination of floating mats of seagrass wrack and the macroalgae *Sargassum* in coastal waters of Greater Florida Bay using airborne remote sensing. *Remote Sensing of Environment* **167**: 247–258. DOI: http://dx.doi.org/10.1016/j.rse.2015.01.027.

Dwyer, RG, **Bearhop, S**, **Campbell, HA**, **Bryant, DM.** 2013. Shedding light on light: Benefits of anthropogenic illumination to a nocturnally foraging shorebird. *Journal of Animal Ecology* **82**(2): 478–485. DOI: https://doi.org/10.1111/1365-2656.12012.

Egbert, GD, **Erofeeva, SY.** 2002. Efficient inverse modeling of barotropic ocean tides. *Journal of Atmospheric and Oceanic Technology* **19**(2): 183–204. DOI: http://dx.doi.org/10.1175/1520-0426(2002)019<0183:Eimobo>2.0.Co;2.

Falchi, F, **Cinzano, P**, **Duriscoe, D**, **Kyba, CCM**, **Elvidge, CD**, **Baugh, K**, **Portnov, BA**, **Rybnikova, NA**, **Furgoni, R.** 2016. The new world atlas of artificial night sky brightness. *Science Advances* **2**(6): e1600377. DOI: http://dx.doi.org/10.1126/sciadv.1600377.

Fobert, EK, **Burke da Silva, K**, **Swearer, SE.** 2019. Artificial light at night causes reproductive failure in clownfish. *Biology Letters* **15**(7): 20190272. DOI: http://dx.doi.org/10.1098/rsbl.2019.0272.

Fobert, EK, **Schubert, KP**, **da Silva, KB.** 2021. The influence of spectral composition of artificial light at night on clownfish reproductive success. *Journal of Experimental Marine Biology and Ecology* **540**: 151559. DOI: http://dx.doi.org/10.1016/j.jembe.2021.151559.

Gaston, KJ, **Ackermann, S**, **Bennie, J**, **Cox, DTC**, **Phillips, BB**, **de Miguel, AS**, **Sanders, D.** 2021. Pervasiveness of biological impacts of artificial light at night. *Integrative and Comparative Biology* **61**(3): 1098–1110. DOI: http://dx.doi.org/10.1093/icb/icab145.

Gerard, VA. 1984. The light environment in a giant-kelp forest: Influence of *Macrocystis pyrifera* on spatial and temporal variability. *Marine Biology* **84**(2): 189–195. DOI: http://dx.doi.org/10.1007/BF00393004.

Gregg, WW, **Carder, KL.** 1990. A simple spectral solar irradiance model for cloudless maritime atmospheres. *Limnology and Oceanography* **35**: 1657–1675.

Hayes, GC. 2003. A review of the adaptive significance and ecosystem consequences of zooplankton diel vertical migrations. *Hydrobiologia* **503**: 163–170.

Jechow, A, **Hölker, F.** 2019. How dark is a river? Artificial light at night in aquatic systems and the need for comprehensive night-time light measurements. *WIREs Water* **6**(6): e1388. DOI: http://dx.doi.org/10.1002/wat2.1388.

Jechow, A, **Kollath, Z**, **Ribas, SJ**, **Spoelstra, H**, **Holker, F**, **Kyba, CCM.** 2017. Imaging and mapping the impact of clouds on skyglow with all-sky photometry. *Scientific Reports* **7**(1): 1–10. DOI: http://dx.doi.org/10.1038/s41598-017-06998-z.

Kronfeld-Schor, N, **Dominoni, D**, **de la Iglesia, H**, **Levy, O**, **Herzog, ED**, **Dayan, T**, **Helfrich-Forster, C.** 2013. Chronobiology by moonlight. *Proceedings of the Royal Society B-Biological Sciences* **280**(1765): 20123088. DOI: http://dx.doi.org/10.1098/rspb.2012.3088.

Kyba, CCM, **Ruhtz, T**, **Fischer, J**, **Holker, F.** 2011. Cloud coverage acts as an amplifier for ecological light pollution in urban ecosystems. *PLoS One* **6**(3): 17307. DOI: http://dx.doi.org/10.1371/journal.pone.0017307.

Last, KS, **Hobbs, L**, **Berge, J**, **Brierley, AS**, **Cottier, F.** 2016. Moonlight drives ocean-scale mass vertical migration of zooplankton during the Arctic winter. *Current Biology* **26**(2): 244–251. DOI: http://dx.doi.org/10.1016/j.cub.2015.11.038.

Lee, ZP, **Carder, KL**, **Arnone, RA.** 2002. Deriving inherent optical properties from water color: A multiband quasi-analytical algorithm for optically deep waters. *Applied Optics* **41**: 5755–5772.

Levy, O, **de Barros Marangoni, LF**, **Benichou, JI**, **Rottier, C**, **Béraud, E**, **Grover, R**, **Ferrier-Pagès, C.** 2020. Artificial light at night (ALAN) alters the physiology and biochemistry of symbiotic reef building corals. *Environmental Pollution* **266**: 114987. DOI: http://dx.doi.org/10.1016/j.envpol.2020.114987.

Ludvigsen, M, **Berge, J**, **Geoffroy, M**, **Cohen, JH**, **De La Torre, PR**, **Nornes, SM**, **Singh, H**, **Sørensen, AJ**, **Daase, M**, **Johnsen, G.** 2018. Use of an autonomous surface vehicle reveals small-scale diel vertical migrations of zooplankton and susceptibility to light pollution under low solar irradiance. *Science Advances* **4**(1): 1–9. DOI: http://dx.doi.org/10.1126/sciadv.aap9887.

Lumme, K, **Bowell, E.** 1981. Radiative-transfer in the surfaces of atmosphereless bodies. 2. Interpretation of

Downloaded from http://online.ucpress.edu/elementa/article-pdf/10/1/00042/765092/elementa.2022.00042.pdf by University of Strathclyde Glasgow user on 13 December 2022

phase curves. *Astronomical Journal* **86**(11): 1705–1721. DOI: http://dx.doi.org/10.1086/113055.

Marangoni, LFB, **Davies, T**, **Smyth, T**, **Rodriguez, A**, **Hamann, M**, **Duarte, C**, **Pendoley, K**, **Berge, J**, **Maggi, E**, **Levy, O.** 2022. Impacts of artificial light at night in marine ecosystems–A review. *Global Change Biology* **28**(18): 5346–5367. DOI: http://dx.doi.org/10.1111/gcb.16264.

McMahon, O, **Smyth, T**, **Davies, TW.** 2022. Broad spectrum artificial light at night increases the conspicuousness of camouflaged prey. *Journal of Applied Ecology* **59**(5): 1324–1333.

Moberg, F, **Folke, C.** 1999. Ecological goods and services of coral reef ecosystems. *Ecological Economics* **29**(2): 215–233. DOI: http://dx.doi.org/10.1016/S0921-8009(99)00009-9.

Mobley, CD. 1994. *Light and water: Radiative transfer in natural waters*. San Diego, CA: Academic Press.

Mobley, CD. 1995. *Hydrolight 3.0 user's guide*. Menlo Park, CA: SRI International.

Naylor, E. 2001. Marine animal behaviour in relation to lunar phase. *Earth Moon and Planets* **85–86**: 291–302.

Neckel, H, **Labs, D.** 1984. The solar radiation between 3300 and 12500A. *Solar Physics* **90**: 205–258.

Payton, L, **Tran, D.** 2019. Moonlight cycles synchronize oyster behaviour. *Biology Letters* **15**(1): 20180299. DOI: http://dx.doi.org/10.1098/rsbl.2018.0299.

Righton, D, **Westerberg, H**, **Feunteun, E**, **Okland, F**, **Gargan, P**, **Amilhat, E**, **Metcalfe, J**, **Lobon-Cervia, J**, **Sjoberg, N**, **Simon, J**, **Acou, A**, **Vedor, M**, **Walker, A**, **Trancart, T**, **Bramick, U**, **Aarestrup, K.** 2016. Empirical observations of the spawning migration of European eels: The long and dangerous road to the Sargasso Sea. *Science Advances* **2**(10): e1501694. DOI: http://dx.doi.org/10.1126/sciadv.1501694.

Roberts, EM, **Bowers, DG**, **Davies, AJ.** 2018. Tidal modulation of seabed light and its implications for benthic algae. *Limnology and Oceanography* **63**(1): 91–106. DOI: http://dx.doi.org/10.1002/lno.10616.

Sanders, D, **Frago, E**, **Kehoe, R**, **Patterson, C**, **Gaston, KJ.** 2021. A meta-analysis of biological impacts of artificial light at night. *Nature Ecology & Evolution* **5**(1): 74–81. DOI: http://dx.doi.org/10.1038/s41559-020-01322-x.

Sathyendranath, S, **Brewin, RJW**, **Brockmann, C**, **Brotas, V**, **Calton, B**, **Chuprin, A**, **Cipollini, P**, **Couto, AB**, **Dingle, J**, **Doerffer, R**, **Donlon, C**, **Dowell, M**, **Farman, A**, **Grant, M**, **Groom, S**, **Horseman, A**, **Jackson, T**, **Krasemann, H**, **Lavender, S**, **Martinez-Vicente, V**, **Mazeran, C**, **Mélin, F**, **Moore, TS**, **Müller, D**, **Regner, P**, **Roy, S**, **Steele, CJ**, **Steinmetz, F**, **Swinton, J**, **Taberner, M**, **Thompson, A**, **Valente, A**, **Zühlke, M**, **Brando, VE**, **Feng, H**, **Feldman, G**, **Franz, BA**, **Frouin, R**, **Gould, RW**, **Hooker, SB**, **Kahru, M**, **Kratzer, S**, **Mitchell, BG**, **Muller-Karger, FE**, **Sosik, HM**, **Voss, KJ**, **Werdell, J**, **Platt, T.** 2019. An ocean-colour time series for use in climate studies: The experience of the ocean-colour climate change initiative (OC-CCI). *Sensors* **19**(19): 4285.

Smyth, TJ, **Wright, AE**, **McKee, D**, **Tidau, S**, **Tamir, R**, **Dubinsky, Z**, **Iluz, D**, **Davies, TW.** 2021. A global atlas of artificial light at night under the sea. *Elementa: Science of the Anthropocene* **9**(1): 00049. DOI: http://dx.doi.org/10.1525/elementa.2021.00049.

Spitschan, M, **Aguirre, GK**, **Brainard, DH**, **Sweeney, AM.** 2016. Variation of outdoor illumination as a function of solar elevation and light pollution. *Scientific Reports* **6**: 26756. DOI: http://dx.doi.org/10.1038/srep26756.

Tamir, R, **Lerner, A**, **Haspel, C**, **Dubinsky, Z**, **Iluz, D.** 2017. The spectral and spatial distribution of light pollution in the waters of the northern Gulf of Aqaba (Eilat). *Scientific Reports* **7**: 42329–42329. DOI: http://dx.doi.org/10.1038/srep42329.

Tidau, S, **Smyth, T**, **McKee, D**, **Wiedenmann, J**, **D'Angelo, C**, **Wilcockson, D**, **Ellison, A**, **Grimmer, AJ**, **Jenkins, SR**, **Widdicombe, S**, **Queiros, AM**, **Talbot, E**, **Wright, A**, **Davies, TW.** 2021. Marine artificial light at night: An empirical and technical guide. *Methods in Ecology and Evolution* **12**(9): 1588–1601. DOI: http://dx.doi.org/10.1111/2041-210x.13653.

Torres, D, **Tidau, S**, **Jenkins, S**, **Davies, T.** 2020. Artificial skyglow disrupts celestial migration at night. *Current Biology* **30**(12): R696–R697. DOI: http://dx.doi.org/10.1016/j.cub.2020.05.002.

Ugolini, A, **Hoelters, LS**, **Ciofini, A**, **Pasquali, V**, **Wilcockson, DC.** 2016. Evidence for discrete solar and lunar orientation mechanisms in the beach amphipod, *Talitrus saltator* Montagu (Crustacea, Amphipoda). *Scientific Reports* **6**: 1–8. DOI: http://dx.doi.org/10.1038/srep35575.

Underwood, CN, **Davies, TW**, **Queirós, AM.** 2017. Artificial light at night alters trophic interactions of intertidal invertebrates. *Journal of Animal Ecology* **86**(4): 781–789. DOI: http://dx.doi.org/10.1111/1365-2656.12670.

United Nations. 2019. *World urbanization prospects: The 2018 revision (ST/ESA/SER.A/420)*. New York, NY: United Nations, Department of Economic and Social Affairs, Population Division.

West, G. 2018. *Scale: The universal laws of life and death in organisms, cities and companies*. London, UK: Weidenfield & Nicholson.

Witherington, BE, **Bjorndal, KA.** 1991. Influences of artificial lighting on the seaward orientation of hatchling loggerhead turtles *Caretta caretta*. *Biological Conservation* **55**(2): 139–149. DOI: http://dx.doi.org/10.1016/0006-3207(91)90053-C.

Yu, X. 2019. Optical properties of turbid coastal water and their remote sensing retrievals based on radiative transfer approaches [PhD dissertation]. Enschede, the Netherlands: University of Twente, Faculty of Geo-Information Science and Earth Observation (ITC).

Downloaded from http://online.ucpress.edu/elementa/article-pdf/10/1/00042/765092/elementa.2022.00042.pdf by University of Strathclyde Glasgow user on 13 December 2022

Downloaded from http://online.ucpress.edu/elementa/article-pdf/10/1/00042/765092/elementa.2022.00042.pdf by University of Strathclyde Glasgow user on 13 December 2022

How to cite this article: Smyth, TJ, Wright, AE, Edwards-Jones, A, McKee, D, Queirós, A, Rendon, O, Tidau, S, Davies, TW. 2022. Disruption of marine habitats by artificial light at night from global coastal megacities. *Elementa: Science of the Anthropocene* 10(1). DOI: https://doi.org/10.1525/elementa.2022.00042

Domain Editor-in-Chief: Jody W. Deming, University of Washington, Seattle, WA, USA

Associate Editor: Kevin Arrigo, Department of Earth System Science, Stanford University, Stanford, CA, USA

Knowledge Domain: Ocean Science

Published: December 1, 2022 **Accepted:** November 4, 2022 **Submitted:** March 12, 2022

Copyright: © 2022 The Author(s). This is an open-access article distributed under the terms of the Creative Commons Attribution 4.0 International License (CC-BY 4.0), which permits unrestricted use, distribution, and reproduction in any medium, provided the original author and source are credited. See http://creativecommons.org/licenses/by/4.0/.

ELEMENTA Science of the Anthropocene

Elem Sci Anth is a peer-reviewed open access journal published by University of California Press.

OPEN ACCESS